*Met. Mater. Int., Vol. 18, No. 6 (2012), pp. 917~921*
doi: 10.1007/s12540-012-7002-3

# Role of Spheroidized Carbides on the Fatigue Life of Bearing Steel

**Kwan-Ho Kim*, Su-Dong Park, Jae-Hwan Kim, and Chul-Min Bae**

Technical Research Laboratories, POSCO, 1 Goedong-dong Nam-gu, Pohang,
Gyeongbuk 790-785, Korea

(received date: 31 October 2011 / accepted date: 10 January 2012)

The fatigue characteristics of bearing steel in ultrasonic fatigue tests are investigated with regard to the role of spheroidized carbides. The results show that, despite a similar hardness level, the bearing steel with spheroidized carbide has a much longer fatigue life than steel without, and that the failure mechanism differs in each case. All the samples of SAQT-processed steel examined using ultrasonic fatigue tests were characterized by a conventional fish-eye structure, which implies they went through subsurface-originated or interior inclusion-induced failure. On the contrary, it was shown that surface-induced failure prevailed in the QT-processed steel without spheroidized carbide. The results suggest spheroidized carbide may strengthen the tempered martensitic matrix of the bearing steel and concentrate the stress around an inclusion rather than at the surface, allowing for prolonged fatigue life over the steel without spheroidized carbide.

**Key words:** fatigue, bearing steel, annealing, microstructure, ultrasonics

## 1. INTRODUCTION

Bearing steels for the rolling parts of automobiles and industrial machinery are required to possess excellent surface hardness for wear, fatigue resistance, and microstructural stability under temperature extremes [1,2]. In this regard, cementite is widely regarded as an essential phase in high carbon chromium bearing steel for two reasons: it usually provides good wear resistance, and acts as a reservoir for alloys, enabling bearing steel to develop the desired properties during heat treatment [3,4]. After hot rolling into wires or bars, bearing steel is subjected to spheroidization annealing to change the pearlitic microstructure into a mixed structure in which spherical cementite particles are uniformly dispersed throughout the ferrite matrix [5]. During the spheroidizing of steels with an initial pearlite structure, the cementite lamellae change their shapes into spherical particles as shown in Fig. 1. This occurs because the surface energy in a structure with a smaller interfacial area, such as the spherical cementite particles in a ferritic matrix, is more stable than in the pearlitic lamellar structure with a larger ferrite/cementite interfacial area [6,7]. After the spheroidization annealing and forging processes, the materials go through a final heat treatment of quenching and tempering to create favorable properties.

It has been reported that, of the various methods of enhancing the fatigue life of bearing steels, increasing the silicon content can increase the hardenability moderately and strengthen quenched and tempered steels, leading to higher resistance against softening during tempering [8,9]. However, increasing the silicon content retarded the spheoridization of cementite, and the thermodynamic calculations revealed that the shrinkage of the austenite phase field in bearing steels as the silicon content increased gives rise to an increase in the volume fraction of cementite at the annealing temperature, possibly resulting in incomplete spheroidization. Furthermore, due to the low solubility of silicon in cementite, an increase in silicon content can raise the activity or chemical potential of carbon atoms in austenite at austenite/cementite interfaces. Consequently, the difference in chemical potential of carbon atoms at the interfaces would decrease as the silicon content increases, causing a decrease in driving force for the diffusion of carbon atoms from cementite to austenite [8-10].

In general, the spheroidization annealing of bearing steel is set up for two purposes. One is to lower the hardness of the bearing steel so that subsequent forging processes can be performed without difficulty [11], and the other is to create a microstructure in which spherical carbides are uniformly dispersed throughout the matrix that they strengthen [12]. Despite the effectiveness of the spheroidized carbides, it is unknown how they contribute to the longer fatigue life of bearing steel. In this study, by investigating bearing steel with and without spheroidized carbides and the difference in their fatigue properties, the role of spheroidized carbides on the fatigue life of bearing steel is discussed.

*Corresponding author: rockite@posco.com

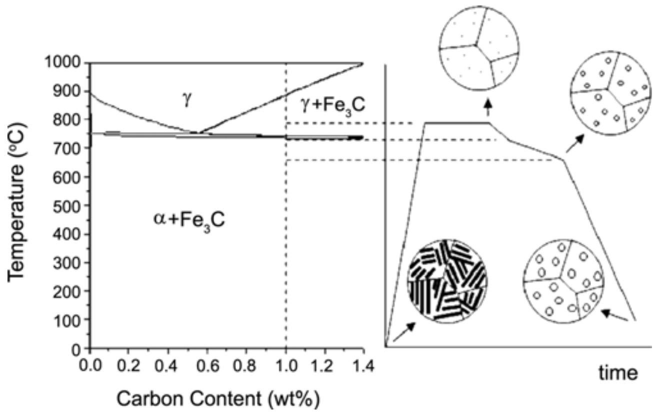


**Fig. 1.** Schematic illustration of spheroidization annealing of bearing steels. Cementites change their shapes from lamellae into seeds and spherical particles in turn.

## 2. EXPERIMENTAL PROCEDURES

The material used in this study is a high-carbon chromium bearing steel, some examples being: 100Cr6, AISI 52100, and SUJ2. The nominal chemical composition of the steel is 1.00C-0.25Si-0.35Mn-1.45Cr in wt% as given in Table 1. After being hot rolled into a wire 16 mm in diameter, specimens for ultrasonic fatigue tests were machined and processed in two different ways. One process was the conventional SAQT (Spherodization Annealing, Quenching and Tempering) process, which implies spheroidization annealing followed by quenching and tempering to form spheroidized carbides within the matrix. The other is the QT (Quenching and Tempering) process, which implies direct quenching and tempering without spheroidization annealing to create whole tempered martensitic microstructures without any spheroidized carbide. The spheroidization annealing was performed by heating the steel at 790 °C for 6 h, and to austenitize the steel before quenching and tempering, the steel was heated at 840 °C for 1 h, allowing spheroidized carbides to remain.

After being quenched and tempered, the fatigue properties of the steel types were evaluated by ultrasonic fatigue tests and analyzed by using Weibull distribution. The specimen shape for the tests is shown in Fig. 2. 24 specimens were tested for each steel type. The circular reduction of the cross-sectional area in the centers of the specimens serves to magnify the strain amplitude. The specimens were ground with a grinding disc to produce close to real surface conditions.

Ultrasonic fatigue tests were performed on the newly developed system with a frequency of 20 kHz and stress ratio $R = -1$ at room temperature [13]. The new system consists of a generator, transducer, horn and computer along with software. A power generator transforms 50 or 60 Hz voltage signal into an ultrasonic 20 kHz electrical sinusoidal signal by means of a piezoelectric transducer. A piezoelectric transducer excited by the power generator transforms the electrical signal into longitudinal ultrasonic waves and mechanical vibration of the same frequency. An ultrasonic horn is attached to the converter mechanically (using a screw) to amplify the vibration coming from the transducer in order to obtain the required strain amplitude in the specimen. A computer along with software automatically controls the ultrasonic fatigue device, and parameters such as strain, stress, and the number of cycles (time to failure) are recorded. Detection of fatigue failure automatically stops the test. The longitudinal displacement on horn end is monitored through a photonic sensor, and finally, a cooler prevents the specimen from heating and maintains ambient temperature during the test. As high strain rate deformation is known to cause a temperature rise due to internal frictional energy loss, ultrasonic fatigue tests were carried out in a pulse-pause manner to minimize this kind of internal friction-induced temperature rise. A software-controlled pulse length of 300 ms and pause time of 600 ms were used. The influence of pulse-pause loading on the fatigue strength of the bearing steel was negligible.

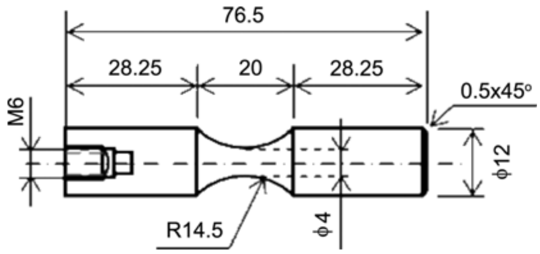


**Fig. 2.** Specimen for ultrasonic fatigue tests. All dimensions are in mm.

Microstructural analyses of the specimen were carried out using a JEOL JSM-7000F field-emission scanning electron microscope equipped with EDS and WDS. The Vickers hardness of all specimens was measured using the Mitutoyo automatic microhardness testing system HV114 with a load of 1 kg. The hardness presented is the average of at least 10 values.

## 3. RESULTS AND DISCUSSION

The microstructural evolution through quenching and tempering with or without spheroidization annealing before ultrasonic fatigue tests is given in Fig. 3. It can be easily confirmed that the conventional SAQT process produces tempered martensite with uniformly-dispersed spheroidized carbides in Fig. 3(a), while QT process only tempered martensite with-

**Table 1.** Chemical composition (mass %) of the steel used in the study

| Alloy | C | Si | Mn | P | S | Cr | Ti | O (ppm) |
|---|---|---|---|---|---|---|---|---|
| 100Cr6 | 0.99 | 0.26 | 0.34 | 0.011 | 0.005 | 1.43 | 0.001 | 4 |

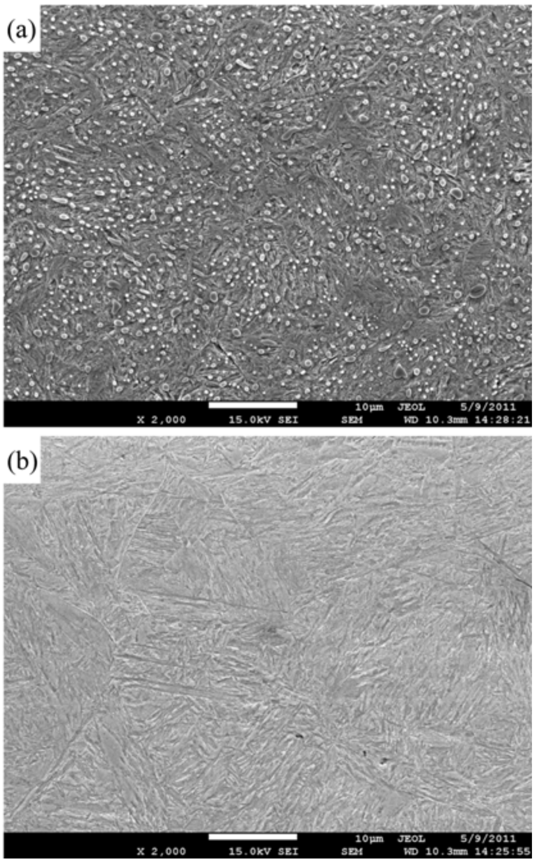


**Fig. 3.** SEM micrographs of (a) SAQT- and (b) QT-processed steels.

**Table 2.** Comparison of hardness of SAQT- and QT-processed steels

| Samples | Position | Hardness (HRC) |
|---|---|---|
| SAQT-processed | Surface | 61.7 |
| | 1/4D | 61.5 |
| QT-processed | Surface | 61.8 |
| | 1/4D | 61.1 |

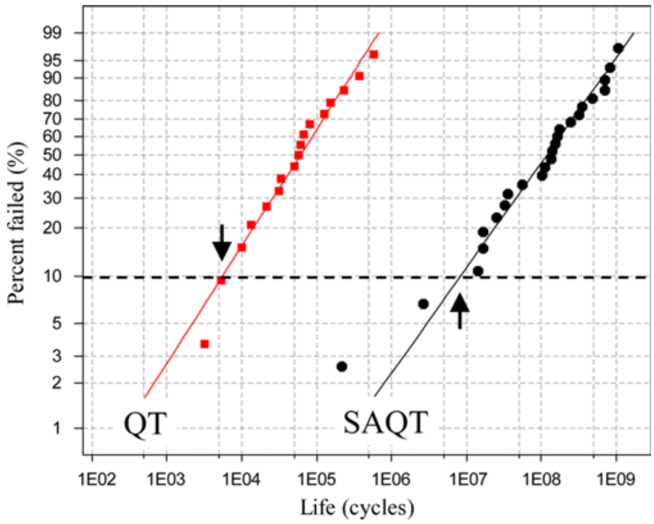


**Fig. 4.** Comparison of fatigue life of the steels measured by ultrasonic fatigue tests.

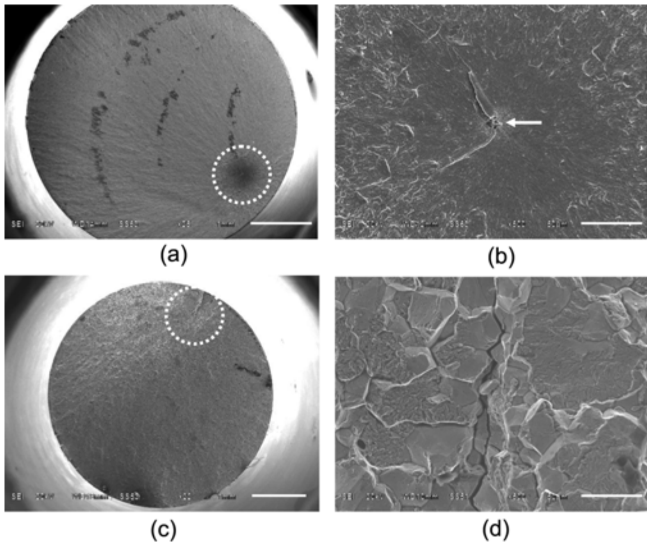


**Fig. 5.** SEM micrographs showing the fracture surfaces of (a) SAQT- and (c) QT-processed steels. (b) and (d) are the enlarged images of dotted region in (a) and (c), respectively.

out spheroidized carbides in Fig. 3(b). The average volume fraction of spheroidized carbides in the SAQT samples was measured to be 3.38% using an image analyzer. Despite the different microstructures, the hardness level was measured to be almost the same, ranging 61.1–61.8 HRC, as demonstrated in Table 2. Generally, bearing steel requires hardness greater than 58 HRC and, therefore, both processes meet the qualifications. It is common for the fatigue life of bearing steel to be dependent upon its hardness.

The fatigue life of the steel measured by ultrasonic fatigue tests is illustrated in Fig. 4. The fatigue life of bearing steel is usually expressed by $L_{10}$, the number of cycles until 10% of samples fail. Compared to the QT process without spheroidization annealing, the SAQT process has much longer fatigue life as marked by arrows in Fig. 4. $L_{10}$ fatigue life is about $8.26 \times 10^6$ for the SAQT-processed steel and $5.50 \times 10^3$ for the QT-processed one, respectively. Considering the same level of hardness, the large difference of fatigue life between two processes may be only attributed to the presence of spheroidized carbides.

In order to clarify the effect of spheroidized carbides on the fatigue life of bearing steel, the fracture surfaces of samples were analyzed as shown in Fig. 5. A typical fish-eye structure, noted as the dotted region in Fig. 5(a), is observed inside the fracture surface of the SAQT-processed specimen such that the fish-eye does not contact with the specimen surface, which implies the fracture is subsurface-originated. As reported earlier [14-16], a nonmetallic inclusion exists at the center of fish-eye structure, marked by an arrow in Fig.

5(b) and identified as $Al_2O_3$ in this study. Furthermore, according to Figs. 5(a) and 5(b), the entire fracture surface can be divided into three regions. The first one is in most interior around the inclusion and has a smooth and flat surface in Fig. 5(b). The second one is the darkest area as marked by the dotted circle in Fig. 5(a) and outside the initial smooth area in Fig. 5(b), which has a rough surface. The third area is a wide fracture surface outside the dotted circle in Fig. 5(a), which has lots of radial streaks indicating crack propagation direction. On the other hand, any distinctive features such as the fish-eye structure and three different regions are not found in the fracture surface of the QT-processed steel as given in Figs. 5(c) and 5(d). Moreover, it is clearly observed that the crack initiates at the surface of specimen without any inclusion and propagates to the interior as marked by the dotted circle. It should be noted, consequently, that the fatigue crack is subsurface-originated in the SAQT-processed steel and surface-originated in the QT-processed one.

Since all the samples of SAQT-processed steel examined by ultrasonic fatigue tests were characterized by conventional fish-eye structure, what kind of nonmetallic inclusions caused such a failure was analyzed as given in Fig. 6. Of total 24 samples tested, 14 were related with TiN and the rest with $Al_2O_3$, respectively. Furthermore, it was confirmed that the fatigue life of bearing steel decreased as the inclusion size increased.

Since the hardness was measured to be almost the same for the two differently processed steels, the difference in fatigue mechanisms between them could only result from the microstructural discrimination; namely the presence of spheroidized carbides. In general, the microstructure of the conventionally SAQT-processed steel consists of tempered martensite, spheroidized carbides, and nonmetallic inclusions such as TiN and $Al_2O_3$, the hardness of which is about 700, 1000, 2000~2500 HV in turn [17]. Because the hardness of spheroidized carbides is higher than that of tempered martensite, they would strengthen the matrix and the grain boundaries, therefore the vibrating force during ultrasonic fatigue tests must be concentrated around an inclusion of much higher hardness [18]. Accordingly, the fatigue crack should initiate at the interface between the matrix and inclusion as shown in Fig. 7(a). The resulting fracture surface features transgranular cleavage as shown in Fig. 5(b). In general, carbides are classified as spherical only when their aspect ratio is smaller than 2.0 because ones with larger aspect ratio than that, such as proeutectoid cementites, do not help additionally strengthen the matrix but instead are detrimental to the fatigue characteristics of bearing steel.

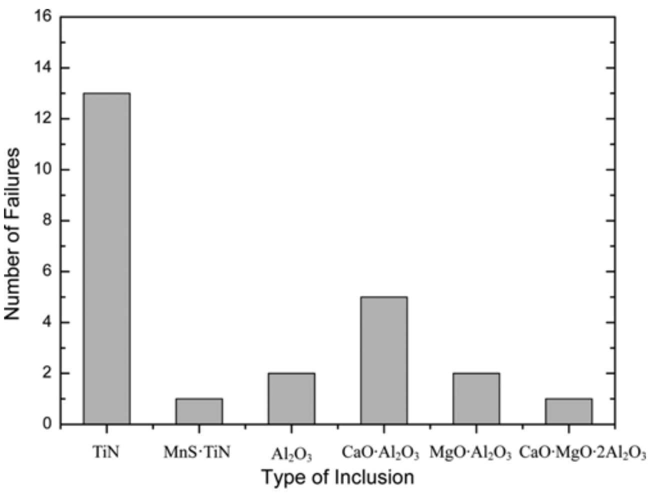


**Fig. 6.** Nonmetallic inclusions causing the failure of SAQT-processed steel during ultrasonic fatigue tests.

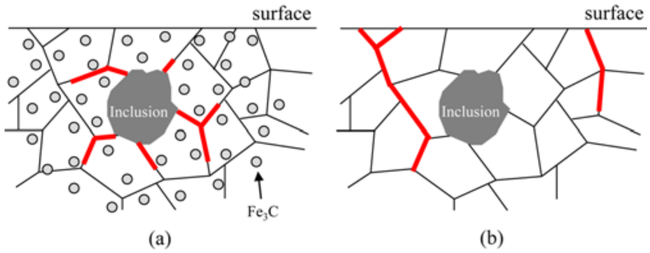


**Fig. 7.** Schematic illustration of fatigue mechanisms of bearing steels (a) with spheroidized carbides and (b) without them. The crack initiation and propagation paths supposed to occur are expressed as thick lines.

On the contrary, as the QT-processed steel has a microstructure of only tempered martensite and inclusions, the matrix of tempered martensite and the grain boundaries cannot be strengthened by spheroidized carbides. For this reason, the vibrating force more easily concentrates on the surface of the specimen than at the interface between the matrix and inclusion. Accordingly, the fatigue crack would initiate at the surface of the specimen and propagate along the grain boundaries as given in Fig. 7(b), and the resulting fracture surface is featured by intergranular separation as shown in Fig. 5(d).

## 4. CONCLUSIONS

The fatigue characteristics of bearing steel have been investigated with regard to the role of spheroidized carbides by ultrasonic fatigue tests and several conclusions are drawn as follows:

(1) Despite a similar hardness level, the bearing steel with spheroidized carbides has much longer fatigue life than the steel without spheroidized carbides. $L_{10}$ fatigue life is about $8.26 \times 10^6$ for the SAQT-processed steel and $5.50 \times 10^3$ for the QT-processed one, respectively.

(2) All the samples of failure in the SAQT-processed steel examined by ultrasonic fatigue tests were characterized by a conventional fish-eye structure, which implies they went through subsurface-originated or interior inclusion-induced

failure. On the contrary, it was shown that surface-induced failures prevailed in the QT-processed steel without spheroidized carbides.

(3) Results suggest that spheroidized carbides serve to strengthen the tempered martensitic matrix, causing stress to concentrate around an inclusion rather than on the surface, prolonging the fatigue life over the steel without spheroidized carbides.

## REFERENCES

1. T. Harris and M. Kotzalas, *Essential Concepts of Bearing Technology, 5th ed.*, pp.277-327, Taylor & Francis, Boca Raton (2007).
2. B. Y. Choi, *Korean J. Met. Mater.* **48**, 1103 (2010).
3. G. Krauss, *Principles of Heat Treatment of Steel*, pp.103-115, Metals Park, Ohio (1980).
4. K. Monma, R. Maruta, T. Yamamoto, and Y. Wakikado, *J. Japan Inst. Metals* **32**, 1198 (1968).
5. K. E. Thelning, *Steel and Its Heat Treatment*, pp.207-216, Butterworth and Co. London (1984).
6. S. Chattopadhyay and C. M. Sellars, *Acta Metall.* **30**, 157 (1982).
7. D. Hernandez-Silva, R. D. Morales, and J. G. Cabanas-Moreno, *ISIJ Int.* **32**, 1297 (1992).
8. K. H. Kim and J. S. Lee, *Mater. Sci. Tech.* **28**, 50 (2012).
9. J. Y. Chae, J. H. Jang, G. Zhang, K. H. Kim, J. S. Lee, H. K. D. H. Bhadeshia, and D. W. Suh, *Scripta Mater.* **65**, 245 (2011).
10. K. H. Kim, J. S. Lee, and D. L. Lee, *Met. Mater. Int.* **16**, 871 (2010).
11. W. Knorr and H. Vöge, in: *Steel. A Handbook for Materials Research and Engineering*, Vol.1, pp.589-603, Verein Deutscher Eisenhüttenleute, Düsseldorf (1992).
12. J. M. Beswick, *Metall. Trans. A* **18**, 1897 (1987).
13. I. S. Cho, A. Amanov, K. H. Kim, C. S. Lee, Y. S. Pyoun, and I. G. Park, *Proc. 5th Int. Conf. on Very High Cycle Fatigue* (eds. C. Berger and H. J. Christ), p.195, German Association for Materials Research and Testing (DVM), Berlin, Germany (2011).
14. T. Sakai, B. Lian, M. Takeda, K. Shiozawa, N. Oguma, Y. Ochi, M. Nakajima, and T. Nakamura, *Int. J. Fatigue* **32**, 497 (2010).
15. T. Sakai, Y. Sato, Y. Nagano, M. Takeda, and N. Oguma, *Int. J. Fatigue* **28**, 1547 (2006).
16. N. Oguma and T. Sakai, *J. Soc. Mat. Sci. Japan* **50**, 516 (2001).
17. ASM Handbook, Friction, Lubrication, and Wear Technology, pp.184-190, ASM Int., Materials Park, Ohio (1992).
18. ASM Handbook, Fatigue and Fracture, pp.42-60, ASM Int., Materials Park, Ohio (1996).